Research Article | Vol. 27, No. 10 | 13 May 2019 | OPTICS EXPRESS 15007
Optics EXPRESS

Demonstration of slow-light effect in silicon-wire waveguides combined with metamaterials

TOMOHIRO AMEMIYA,[1,2,*] SATOSHI YAMASAKI,[1] MAKOTO TANAKA,[1] HIBIKI KAGAMI,[1] KEISUKE MASUDA,[1] NOBUHIKO NISHIYAMA,[1] AND SHIGEHISA ARAI [1,2]

[1] *Institute of Innovative Research (IIR), Tokyo Institute of Technology, Tokyo 152-8552, Japan*
[2] *Department of Electrical and Electronic Engineering, Tokyo Institute of Technology, Tokyo 152-8552, Japan*
**amemiya.t.ab@m.titech.ac.jp*

Abstract: We demonstrated a novel slow-light Si-wire waveguide combined with metamaterials, which can be easily integrated with other Si photonics devices. The slow-light effect can be produced simply by placing metamaterials at an appropriate position on a Si-wire waveguide. It was confirmed that the large group index of more than 40 could be obtained because of a steep and discontinuous change of dispersion relation near the resonance frequency of metamaterials.

1. Developing optical delay line for silicon photonic integrated circuits

1.1 Metamaterial opening new fields of optics

The metamaterial is an artificial material designed to control electric permittivity and magnetic permeability freely beyond naturally existing values. It is an assembly of periodically arranged multiple nanostructural elements, such as sub-wavelength ring resonators smaller than half the wavelength of light, that interact with the electromagnetic field of light.

The metamaterial can exhibit extraordinary optical properties not existing in nature. The topic that has been drawing particular attention is ‘negative refractive index,’ which can be achieved by setting both permittivity and permeability negative. It is predicted that using such unique property enables to create novel optical devices such as a super lens with resolution exceeding the diffraction limit and an optical shielding cloak making objects invisible. The possibility of such sophisticated control on optical waves has had a great influence on 'spatial optics' and 'waveguide optics.'

Spatial optics is one branch of optics applied to the fields of display, imaging, femtosecond laser processing and so on. One of hot topics on the introduction of metamaterials to spatial optics is the metasurface (flat optics) [1] —a technology to freely control the phase distribution of plane waves, using a set of metamaterial elements with appropriate planar layout. On the basis of this concept, several possible applications such as spatial light modulators [2], imaging with ultra-high resolution [3,4], and the invisibility cloak [5] have been reported.

Waveguide optics is another branch of optics applied mainly to photonic integrated circuits (PICs) for optical communication systems [6–8]. Introducing metamaterials to waveguide optics has opened a novel field—‘magnetic permeability design’ for semiconductor waveguides. That is, using metamaterials, the relative permeability of semiconductor waveguides can be controlled freely without being fixed to 1 at optical frequencies. This enables the miniaturization and high performance of existing devices. Furthermore, it make possible to create innovative photonic devices beyond conventional concepts, such as an optical buffer using the effect of optical trapping. A pioneering work in this field was reported in 2003 by Shadrivov *et al.* [9], and in 2007 by K. L. Tsakmakidis *et al.* [10]; they predicted the phenomenon of rainbow trapping (i.e., wavelength-dependent negative Goos-Hänchen shift) in

#360195 https://doi.org/10.1364/OE.27.015007
Journal © 2019 Received 14 Feb 2019; revised 3 Apr 2019; accepted 4 Apr 2019; published 9 May 2019

Optics EXPRESS

a waveguide induced by the negative refractive index of metamaterials. Inspired by this result, various attempts have been made to change the optical properties of semiconductor waveguides using metamaterials consisting of metal nanostructural elements [11,12]. Recently, various applied research has been advanced to create novel photonic devices using a combination of waveguides and metamaterials, such as the "trapped rainbow" light storage [13,14], ultra-compact optical modulators [15], the CPA (coherent perfect absorber)-laser for lasing and anti-lasing [16], the unidirectional mode converters [17], the waveguide-integrated mode-selective nano-antennas [18].

1.2 Optical delay line using slow-light effect

This paper demonstrates an optical delay line for silicon photonic integrated circuit (Si-PICs). This device makes use of the slow light effect induced in the silicon-wire waveguide by metamaterials attached on the waveguide.

The Si-PIC can achieve high density integration and therefore small chip area as compared with other PICs made from silica, polymers, and compound semiconductors. This is because a silicon waveguide can be bent steeply with a small bending radius (< 10 μm) because of a large difference in refractive index between silicon core and SiO_2 cladding. In addition, when manufacturing Si-PICs, we can use silicon nanofabrication technology—a mature technology developed for LSI manufacturing. For these reasons, researches for application of Si-PICs have recently been actively conducted [19,20].

One of the difficult operations in PIC is to delay a signal of light. For advanced signal processing, it is desirable to be able to delay a light signal by an integer multiple of the clock period, to hold a light signal for a predetermined time, and so on. For this purpose, two kind of delay lines—one uses ordinary waveguides and the other uses photonic-crystal waveguides with the slow-light effect [21,22]—have been studied. However, the former requires a long line even for a short delay and therefore significantly increases the chip area. The latter has problems such as large mode mismatch when connected to ordinary Si wire waveguides and large scattering loss in photonic crystal.

To overcome these problems, we previously proposed a method to delay light signals with a silicon-wire waveguide with a metamaterial on the surface [23]. This method makes use of a slow light effect in the waveguide induced by the steep wavelength dispersion of the metamaterial. A large delay of light signal can be achieved simply by attaching a metamaterial to the surface of the waveguide.

On the basis of our previous proposal, we report the embodiment of the silicon-wire waveguide with a metamaterial for use in the 1.55-μm band, and observe the slow-light effect occurring in the waveguide. As the metamaterial, we used an array of sub-wavelength metal-ring resonators. The following sections report the results. Section 2 explains the structure and operation of the device through theoretical analysis. In Section 3, we design the structure of metal-ring resonators that forms the metamaterial, using the experimental results of interaction between light waves and the metal-ring resonator. In Section 4, we make a silicon-wire waveguide with the metamaterial on the surface, and observe the slow-light effect occurred in the waveguide. It is confirmed that the group velocity of light in the waveguide slows down by the presence of the metamaterial. A velocity reduction of one tenth or less can be achieved. The possibility of application to optical delay lines is also discussed.

2. Slow-light effect in Si-wire waveguide with metamaterial: theory

Figure 1a shows the structure of our Si-wire waveguide with a metamaterial. The device consists of a Si core and SiO_2 cladding surrounding the core. A one-dimensional array of sub-wavelength split-ring resonators (SRRs) [24], which operates as a metamaterial, is embedded in the upper cladding. Let us suppose that light with a frequency close to the *LC* resonance frequency of the SRR is traveling through the waveguide. Also suppose that the light has electric field parallel to the gap of the SRR or has magnetic field perpendicular to the SRR

Optics EXPRESS

plane. In this condition, a circulating current is induced in the SRRs and produces a magnetic dipole moment in response to the light. As a result, the effective permeability of SiO_2 cladding near the SRR array is different from the natural value of SiO_2 (= permeability of vacuum). In this paper, we use TE-mode light, and therefore electric field of light is parallel to the gap. In the explanation above, we called the SRR array 'metamaterial,' but to be precise, the metamaterial is a combination of the SRR array and the part of the cladding whose permeability is changed to the effective value.

In ordinary Si-wire waveguides, the dispersion relation is almost linear because the refractive index of Si and SiO_2 are not very dependent on wavelength. In contrast, in the Si-wire waveguide with SRRs (hereafter called the 'SRR waveguide'), the permeability of the SiO_2 cladding changes greatly from its natural value (= μ_0) when the frequency of light approach the resonance frequency of the SRR. This results in a steep and discontinuous change of dispersion relation near the resonance frequency. Figure 1b shows the schematic of such dispersion relation together with light lines for Si and SiO_2. As the slope of the dispersion curve represents the reciprocal of group index, a very large group index (therefore very small group velocity) can be obtained in the vicinity of the resonance frequency.

In the following, the dimensions of SRRs and their placement position in the Si wire waveguide were determined by calculation so as to obtain a large slow light effect in the 1.55-μm band. The method of calculation has reported in [23], and therefore the details of the calculation are not mentioned.

To obtain the dispersion relation of waveguides, it is necessary to solve the wave equation. In a waveguide including a material with anisotropic permittivity and permeability, the wave equation for TE-mode light can be written as [25],

$$\frac{\partial^2 E_x}{\partial y^2} + \left(\omega^2 \varepsilon_0 \mu_0 \varepsilon_x \mu_z - \beta^2 \frac{\mu_z}{\mu_y} \right) E_x = 0, \tag{1}$$

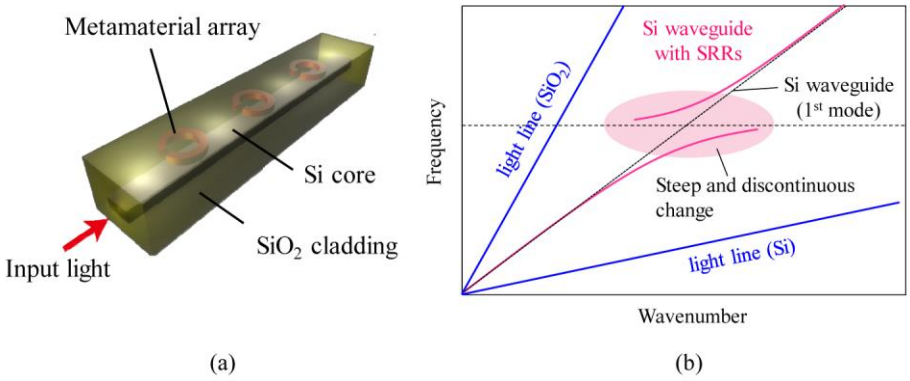

Fig. 1. (a) Schematic of Si-wire waveguide with metamaterials (SRRs). (b) Conceptual image of the dispersion curve of SRR waveguide compared with those of Si, SiO2, and ordinary Si waveguide. Very large group index can be obtained in SRR waveguide because of steep and discontinuous change of dispersion relation near SRR resonance frequency.

where Ex is the electric field component in the x direction, ω is the angular frequency of light, ε_0 is the dielectric constant of the vacuum, μ_0 is the permeability of vacuum, β is the propagation constant of light, and ε_x, μ_y and μ_z are the components of relative-permittivity and relative-permeability tensors. In the SRR waveguide, the values of μ_y and μ_z are not 1 in the SiO_2 cladding near the SRRs.

To solve the wave equation, we divided the waveguide into multiple layers to calculate the spatial dependence of optical field. We also replaced the one-dimensional SRR array and its

Optics EXPRESS

neighboring SiO_2 region with a single uniform layer made of an imaginary material (Fig. 2a). This uniform layer has anisotropy due to the operation of SRRs. The thickness C_2 and width C_1 of the uniform layer are equal to the distance over which the influence of the SRR magnetic dipole extends. With theoretical consideration, we set both thickness C_2 and width C_1 were twice the side length w of the SRR (i.e. $C_2 = C_1$). Next, we determined the equivalent values of ε_x, μ_y and μ_z of the uniform layer, using the method based on S parameters. In this method, a SiO_2 cuboid unit cell (Fig. 2b) containing one SRR is first assumed. The height (thickness) C_2 and width C_1 of the cell are equal to those of the uniform layer, and the length C_3 is equal to the array pitch of SRRs. Then, with the aid of electromagnetic simulation, the S parameters of the cell are calculated for incident plane waves of light introduced along *y* and *z* directions. Finally the values of ε_x, μ_y and μ_z are determined to give the same S parameter when replacing the cell with a cuboid of the imaginary material with the same dimensions. For details on this method, see [26].

In this work, the Si-core width and height of the SRR waveguide were set to 500 nm and 220 nm. We calculated the dispersion relation and group index of the SRR waveguide as a function of distance *h* between the Si core and the uniform layer. Figs. 3 shows one example for h = 100 nm. In this example, the structural parameters of the metal ring (see Fig. 2 b) are set to l = 100 nm, w = 150 nm, a = 30 nm, and d = 50 nm so that resonance will occur at an optical communication frequency. In this paper, we discuss the group refractive index of the SRR waveguide, i.e. the most basic constant in the slow-light effect that occurs in the SRR waveguide. The group refractive index depends on the linear density of SRRs (i.e. the number of SRRs per unit length of the waveguide). If the group index is known, optical signal delay due to the slow-light effect can be calculated from waveguide length. To obtain a large slow-light effect, the SRRs have to be arranged as dense as possible at an interval (or pitch) at which adjacent SRRs cause no magnetic interference with each other. In this paper, we set the pitch to 400 μm with some margin and performed calculation and experiments with this pitch (probably a little bit smaller pitch would do).

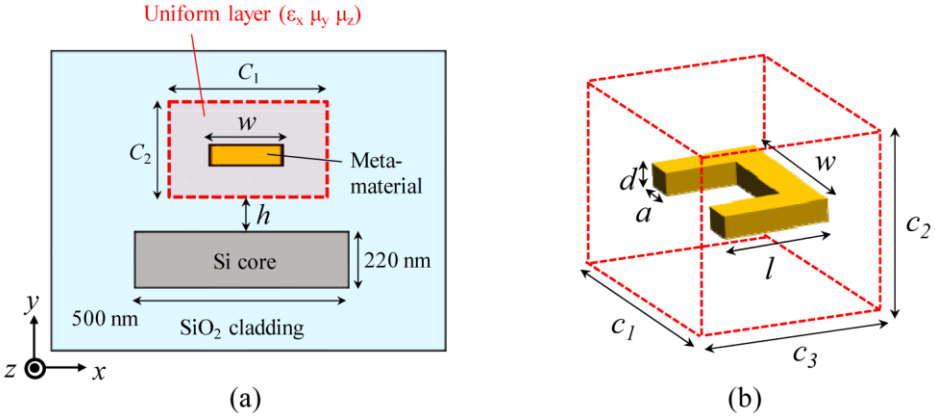

Fig. 2. (a) Cross-section of the Si-wire waveguide combined with metamaterials. One-dimensional SRR array and its neighboring SiO_2 region is replaced with a single uniform layer $C_1 \times C_2 \times C_3$ made of an imaginary material. (b) Structural parameters of the metal ring and its unit cell.

Optics EXPRESS

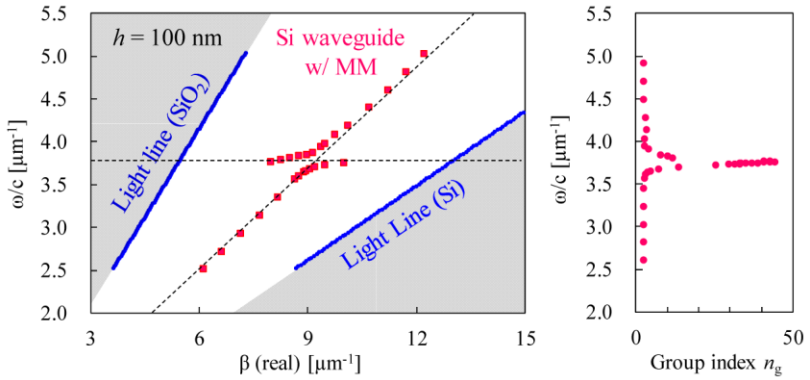

Fig. 3. One example of the dispersion curve and group index of the Si-wire waveguides combined with metamaterials (h = 100 nm in Fig. 2(a)). In this example, the structural parameters of the metamaterial (see Fig. 2 (b)) are set to l = 100 nm, w = 150 nm, a = 30 nm, and d = 50 nm so that resonance will occur at an optical communication frequency.

Two blue lines in the figure show the dispersion relation of light (light line) in Si and SiO_2, and red dots show the calculated dispersion relation of the SRR waveguide. The dispersion relation in the SRR waveguide shows strong nonlinearity and discontinuity in the vicinity of the resonant frequency. This reflects the sharp change in permeability of the SiO_2 cladding. As the slope of the dispersion curve represents the reciprocal of group refractive index, a very large group index is obtained in the vicinity of the resonance frequency. Although loss increases with the SRR resonance, the large group index enables to achieve a practical slow-light, delay line with a loss of 3 dB or less by setting an appropriate device length (see [23]).

From the dispersion relation, we calculated the maximum values of the group index ng and its full width at half maximum (FWHM). Figure 4 shows the results as a function of the distance h between the Si core and the uniform layer. The group index took a maximum value of 44 at h = 100 nm; it is possible to achieve a delay of 44 times compared to a conventional waveguide of the same length. The group index and its FWHM decreased when h was increased from 100 nm because of decrease in interaction between light and SRRs decreased. It is preferable for practical use that a frequency range in which group index becomes large (i.e. a frequency range in which dispersion relation becomes nonlinear) is wide. This frequency range was reduced as the distance between the Si core and the SRR array was decreased. From the results above, we determined to make the SRR waveguide with h = 100 nm.

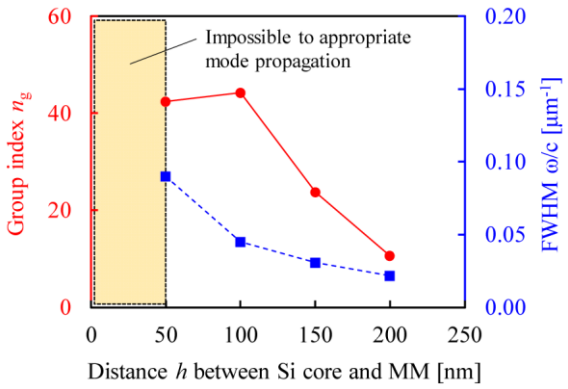

Fig. 4. Calculated maximum values of the group index n_g and its full width at half maximum as a function of distance h between Si core and uniform layer.

Optics EXPRESS

3. Resonance experiment of SRR and 1.55 μm band light

Before making the SRR waveguide, we confirmed by experiment the resonance of the SRR and 1.55-μm band light. To make SRRs for measurement, an Si wafer was used as a starting substrate because it is transparent in the near infrared region. On the Si substrate, a SiO_2 layer of 200-nm thickness was formed using plasma-enhanced chemical vapor deposition (plasma CVD). On its surface, photoresist (polymethylmethacrylate: PMMA) was applied, and the pattern of a two-dimensional SRR array was formed using electron-beam lithography. After that, a Ti layer (10-nm thickness) and an Au layer (40-nm thickness) were deposited in this order, using electron-beam deposition. Then the SRR array consisting of the Ti-Au bilayer was made using lift-off process. Finally, a 200-nm thick SiO_2 layer was deposited using plasma CVD. In the actual SRR waveguide, as shown in the next section, the SRR array is surrounded by SiO_2. Therefore, this experiment was done as well.

In general, in the nanofabrication of sub-wavelength metal rings, an error of about 5 to 10% is inevitable with respect to the design value on CAD. This greatly affect the resonance frequency of the SRR array. To cope with this, SRRs of several sizes were prepared, centering on the original design values. That is, several SRRs with different dimension parameters *l* and *w* within the range of 80-120 nm and 130-170 nm were made on the same substrate. The ring width *a* was fixed at 30 nm. (For *l*, *w*, and *a*, see Fig. 2b). The array pitch of SRRs was set to 400 nm.

To know the resonance characteristic of each SRR, we applied input light from above the SRRs and measured the intensity of the transmitted light. The electric field of the input light was set parallel to the SRR gap. The intensity of transmitted light was measured using Fourier transform infrared spectrometer (FTIR). As shown in Fig. 5a, the transmission intensity varied with the strength of *LC* resonance and became minimum at the resonance wavelength (i.e. frequency at which permeability changes greatly in the vicinity). The resonance wavelength increased with decrease in SRR dimensions (Fig. 5a). Figure 5b shows the measured resonance wavelength as a function of *w* and *l* (A, B and C correspond to each spectrum in Fig. 5(a)). To make the SRR waveguide, we selected three *w*-*l* sets that resonated at 1.51-μm, 1.56-μm, and 1.58-μm wavelengths. The three sets are (i) type 1 (*w* = 130 nm, *l* = 120 nm) for 1.51 μm, (ii) type 2 (*w* = 170 nm, *l* = 90 nm) for 1.56 μm, and (iii) type 3 (*w* = 150 nm, *l* = 120 nm) for 1.58 μm.

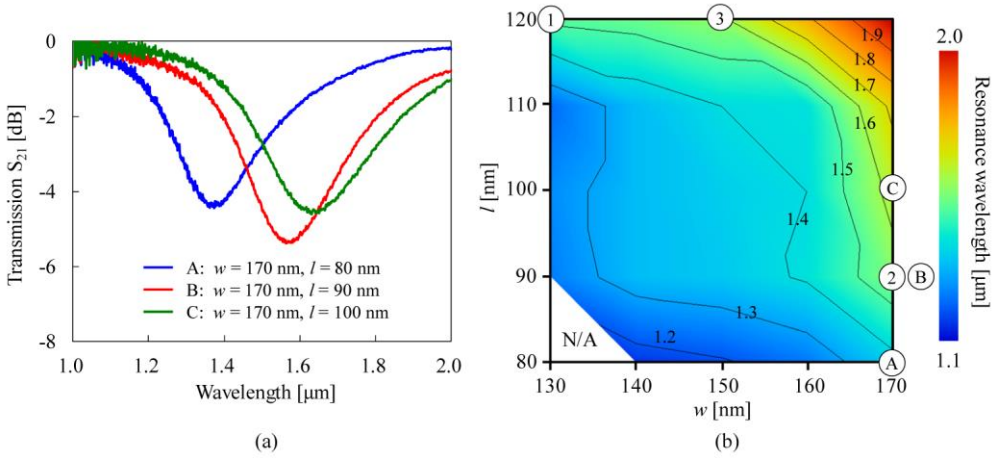

Fig. 5. (a) Normalized FTIR transmission spectra of the SRR array surrounded by SiO_2, measured with different ring size. (b) Measured resonance wavelength as a function of *w* and *l*. A, B and C correspond to each spectrum in Fig. 5(a). N/A means fabrication limit of lift-off process.

Optics EXPRESS

4. Fabrication of SRR waveguides and observation of slow-light effect

We made an actual SRR waveguide and measured the group index of the waveguide (therefore group velocity of light in the waveguide) to confirm the slow-light effect occurred in the waveguide.

The fabrication process of the SRR waveguide is illustrated in Fig. 6. A starting material was a silicon-on-insulator (SOI) substrate with the topmost Si layer of 220-nm thickness. A 200-nm thick SiO_2 layer was formed on the Si surface, using plasma CVD. A Ti-Au SRR array was formed on the surface, using PMMA coating, electron-beam lithography (Fig. 6a), electron-beam deposition, and lift-off process (Fig. 6b). The thickness of Ti and Au were set to 10 nm and 40 nm. Then, a 10-nm thick SiO_2 layer was formed on the surface to protect the SRRs, using plasma CVD (Fig. 6c). After that, a Si-wire waveguide was formed, using ZEP-520 resist coating, electron-beam lithography (Fig. 6d), and CF_4-SF_6 inductively coupled plasma etching (Fig. 6e). Finally, a 1-μm thick SiO_2 layer was formed on the surface (Fig. 6f), and the end faces were exposed with wafer dicing.

We estimated the group index of the SRR waveguide, using an unbalanced Mach-Zehnder Interferometer (MZI) with a difference in optical path length between the two arms. The free spectrum range (FSR) in the transmission spectrum of an unbalanced MZI is proportional to wavelength if the refractive index of the arms is independent of wavelength. In contrast, it shows nonlinear dependence on wavelength if the arms has chromatic dispersion. Making use of this, we can calculate the group index of the part corresponding to the arm length difference. As shown in [27], the group index is given by

$$n_g = \frac{\lambda_{\min} \cdot \lambda_{\max}}{2 \cdot \Delta L \cdot \Delta\lambda}, \tag{2}$$

where $\Delta\lambda$ is FSR, $\lambda_{\min}$ and $\lambda_{\max}$ are the minimum and maximum wavelengths of FSR, and ΔL is the length of the SRR waveguide inserted as part of one arm.

To measure the group index of the SRR waveguide, we made actual unbalanced MZIs consisting of Si-wire waveguides. Figure 7a shows an optical micrograph of the MZI. The SRR waveguide to be measured is added as part of the right arm, so the right arm is longer than the left one by that length. Figure 7b shows a scanning electron microscope image of the SRR waveguide inserted in the right arm.

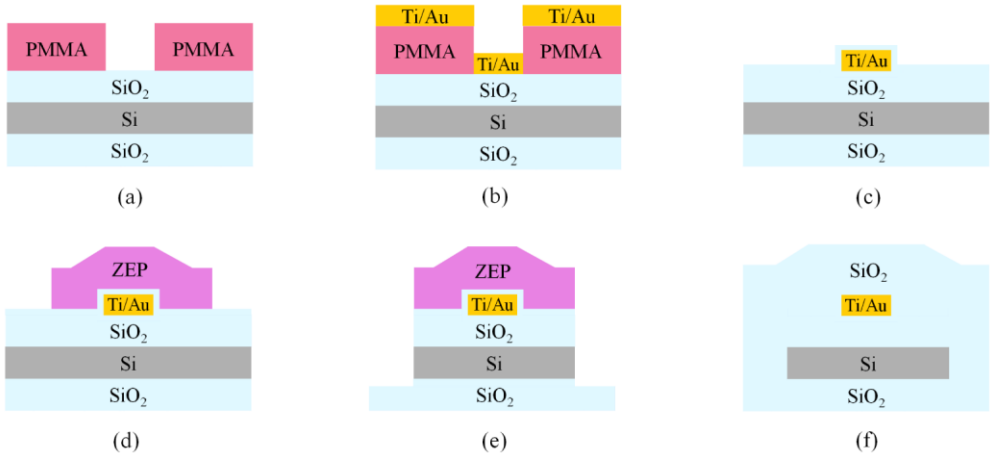

Fig. 6. Fabrication process of the Si-wire waveguide combined with metamaterials.

Optics EXPRESS

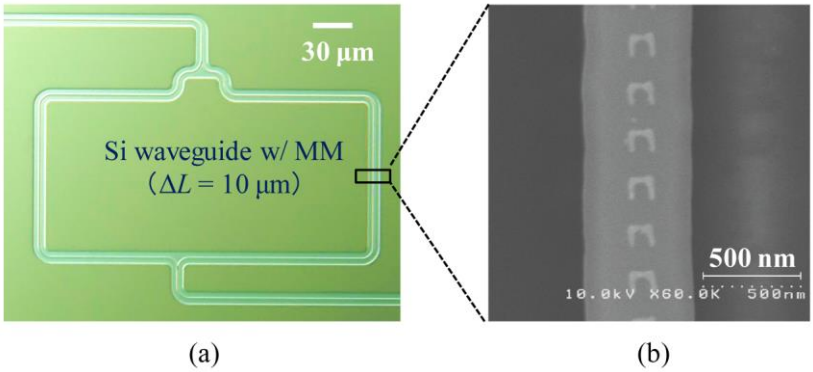

Fig. 7. (a) Optical micrograph of actual unbalanced MZIs consisting of Si-wire waveguides. The SRR waveguide to be measured is added as part of the right arm (ΔL = 10 μm). (b) Scanning electron microscope image of the SRR waveguide inserted in the right arm.

As a control, we first measured the group index of a Si-wire waveguide without SRRs. For this purpose, a MZI with 600-μm arm length difference (ΔL = 600 μm) was made to measure its transmission spectrum. To apply light to the MZI, an amplified spontaneous emission (ASE) light source with a wavelength range of 1530-1610 nm was used. The light from the ASE was fixed to the TE mode using a polarization controller. Figure 8a shows the results. The blue line represents the measured transmission spectrum, and the red points represent the group index at each wavelength obtained from the FSR. The group index was almost constant in this wavelength range and about 4.2. This value is consistent with the result reported in [27].

Next, we measured the group index of the SRR waveguide. As described in Section 3, we prepared SRRs with three different dimensions. Using these SRRs, we made three SRR waveguides, (i) waveguide 1 with type-1 SRRs, (ii) waveguide 2 with type-2 SRRs, and (iii) waveguide 3 with type-3 SRRs. Then, three unbalanced MZIs with each SRR waveguide inserted in the arm were made (see Fig. 7b). Using these MZIs, we measured the group index of SRR waveguides 1, 2, and 3.

Figure 8b shows the result measured for SRR waveguide 2. In this example, the length of the SRR waveguide was set to 10 μm (therefore arm length difference ΔL = 10 μm). The blue line represents the transmission spectrum, and the red points represent the group index at each wavelength calculated from the FSR. As compared to an ordinary Si waveguide (see Fig. 8a), the SRR waveguide showed a large FSR in its transmission spectrum. The group index was obtained to be about 45 in the measurement wavelength range, and it was about 10 times larger than that of an ordinary Si waveguide. Therefore, this SRR waveguide can achieve an optical signal delay of 10 times that of a normal Si waveguide (Unlike TE-mode light, TM-mode light did not produce such results shown in Figs. 8 and 9 because it cannot excite the SRRs).

In the vicinity of wavelength 1575 nm (shown as ‘high loss region’ in Fig. 8b), the transmission spectrum did not change much and FSR was unable to be observed. This wavelength corresponds to the resonance frequency of the SRR, and in the vicinity the absorption loss of light in the waveguide is very large. This made it difficult to distinguish peaks and valleys of the spectrum and therefore to measure FSR. At frequencies very close to the resonance frequency, the SRR waveguide shows a very large group index but cannot be used for practical use because of large absorption loss of light. (The transmission intensity in the vicinity of 1570-1590 nm is reduced by about 5-6 dB because of increasing loss due to resonance. However, the loss is suppressed to some extent because SRRs are separated from the Si core and the length of the SRR waveguide is small).

Optics EXPRESS

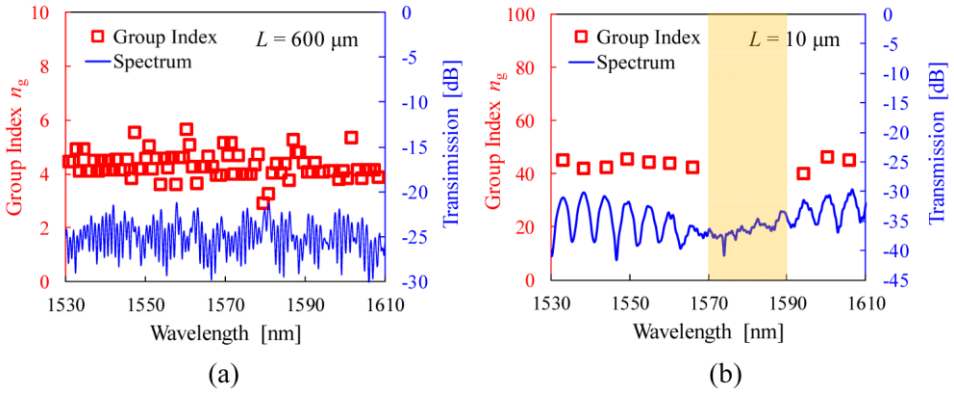

Fig. 8. TE-mode transmission spectra and derived group indices of Si MZIs (a) w/o and (b) w/ metamaterials (Dataset 1, [28]). The blue line represents the measured transmission spectrum, and the red points represent the group index at each wavelength obtained from the FSR.

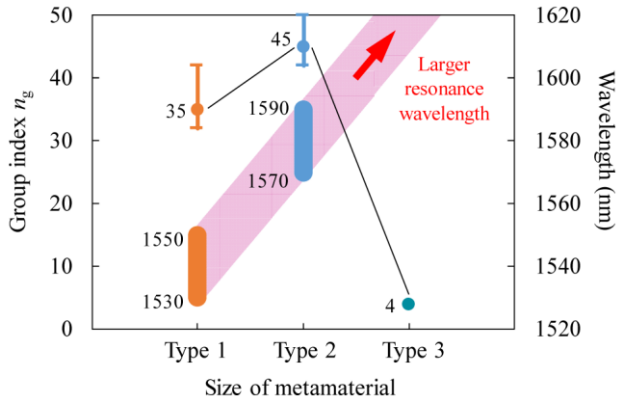

Fig. 9. Summary of the measured group index and the resonance wavelength band of SRR waveguides for each structure.

In the simulation, the group refractive index drops sharply as the wavelength of light moves away from the resonant wavelength. In the experiment, however, the group refractive index remains a high value at wavelengths away from the resonant wavelength. This is probably due to the variation in SRR dimensions. That is, even with one SRR waveguide, there is slight dimensional variation between SRRs formed using the lift-off process. Therefore, the resonance frequency of SRRs also vary. This probably mitigates the extent to which the refractive index decreases as the wavelength of light moves away from the (average) resonance point.

Figure 9 summarizes the group index and the resonance wavelength of SRR waveguides we measured. The group index was 45 in waveguide 1 and 35 in waveguide 2. (For the transmission spectrum and group index of waveguide 1, see Appendix, Fig. 10). The resonance wavelength was 1540 nm in waveguide 1 and 1580 nm in waveguide 2. In waveguide 3, the resonance frequency was outside the measurement frequency range, and therefore the group index did not change so much in the measurement wavelength range.

In all waveguides, the resonance frequency slightly shifted to longer wavelengths compared to the values measured in Section 3. This is because the way of light incidence differed between this measurement and the previous measurement. In the previous section, light was applied perpendicular to the SRR plane using a FTIR microscope, and the SRR was excited only with electric field of light. In contrast, in this measurement, TE-mode light was input to the waveguide (therefore parallel to the SRR plane), and the SRR was excited with both electric

Optics EXPRESS

field and magnetic field of light. This difference produced the slight difference in the resonance frequency.

5. Summary

One promising application of metamaterials is the "slow-light" devices, which can decelerate the group velocity of the guided light waves. In this paper, we have investigated a slow-light Si-wire waveguide combined with metamaterials, which is extremely simple and easier to integrate with other Si photonics devices. We estimated the group index of the device, using an unbalanced MZI with a difference in optical path length between the two arms. For Si-wire waveguide with appropriately designed SRRs, the maximum group index of ~45 was achieved near the resonant wavelength (~1580 nm). This value is 10 times larger than that of the normal Si-wire waveguide w/o metamaterials (n_g ~4.2). In addition, the clear interference fringes were not observed near the wavelength of 1575 nm, which reflects the discontinuity point of the dispersion curve of the device.

Appendix

As a supplement, the transmission spectrum and group index measured for waveguide 1 is shown.

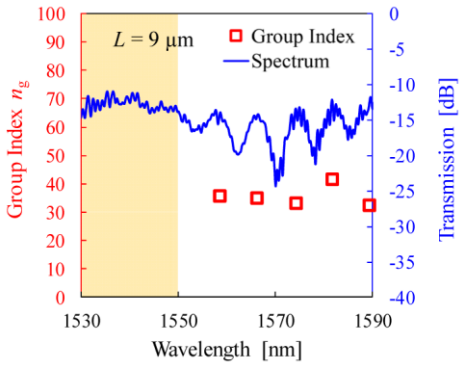

Fig. 10. TE-mode transmission spectra and derived group indices of waveguide 1. The blue line represents the measured transmission spectrum, and the red points represent the group index at each wavelength obtained from the FSR.

Funding

JST-CREST (JPMJCR15N6, JPMJCR18T4) and JSPS KAKENHI (#15H05763, #16H06082).

References

1. N. Yu and F. Capasso, "Flat optics with designer metasurfaces," Nat. Mater. **13**(2), 139–150 (2014).
2. E. Maguid, I. Yulevich, D. Veksler, V. Kleiner, M. L. Brongersma, and E. Hasman, "Photonic spin-controlled multifunctional shared-aperture antenna array," Science **352**(6290), 1202–1206 (2016).
3. Z. Jacob, L. V. Alekseyev, and E. Narimanov, "Optical Hyperlens: Far-field imaging beyond the diffraction limit," Opt. Express **14**(18), 8247–8256 (2006).
4. W. T. Chen, K.-Y. Yang, C.-M. Wang, Y.-W. Huang, G. Sun, I.-D. Chiang, C. Y. Liao, W.-L. Hsu, H. T. Lin, S. Sun, L. Zhou, A. Q. Liu, and D. P. Tsai, "High-efficiency broadband meta-hologram with polarization-controlled dual images," Nano Lett. **14**(1), 225–230 (2014).
5. X. Ni, Z. J. Wong, M. Mrejen, Y. Wang, and X. Zhang, "An ultrathin invisibility skin cloak for visible light," Science **349**(6254), 1310–1314 (2015).
6. R. Nagarajan, C. H. Joyner, R. P. Schneider, Jr., J. S. Bostak, T. Butrie, A. G. Dentai, V. G. Dominic, P. W. Evans, M. Kato, M. Kauffman, D. J. H. Lambert, S. K. Mathis, A. Mathur, R. H. Miles, M. L. Mitchell, M. J. Missey, S. Murthy, A. C. Nilsson, F. H. Peters, S. C. Pennypacker, J. L. Pleumeekers, R. A. Salvatore, R. K. Schlenker, R. B. Taylor, H. S. Tsai, M. F. V. Leeuwen, J. Webjorn, M. Ziari, D. Perkins, J. Singh, S. G. Grubb, M. S. Reffle, D. G. Mehuys, F. A. Kish, and D. F. Welch, "Large-scale photonic integrated circuits," IEEE J. Sel. Top. Quantum Electron. **11**(1), 50–65 (2005).

Optics EXPRESS

7. J. J. G. M. van der Tol, Y. S. Oei, U. Khalique, R. Nötzel, and M. K. Smit, "InP-based photonic circuits: Comparison of monolithic integration techniques," Prog. Quantum Electron. **34**(4), 135–172 (2010).
8. M. R. Watts, J. Sun, E. Timurdogan, E. S. Hosseini, C. Sorace-Agaskar, A. Yaacobi, Z. Su, M. Moresco, and Purnawirman, J. Bradley, G. Leake, T. N. Adam, and D. D. Coolbaugh, "Very Large Scale Integrated Photonics (VLSI-P)," *Proc. CLEO 2014*, SM4O.4 (2014).
9. I. V. Shadrivov, A. A. Sukhorukov, and Y. S. Kivshar, "Guided modes in negative-refractive-index waveguides," Phys. Rev. E Stat. Nonlin. Soft Matter Phys. **67**(5 Pt 2), 057602 (2003).
10. K. L. Tsakmakidis, A. D. Boardman, and O. Hess, "'Trapped rainbow' storage of light in metamaterials," Nature **450**(7168), 397–401 (2007).
11. T. Amemiya, T. Shindo, D. Takahashi, N. Nishiyama, and S. Arai, "Magnetic Interactions at Optical Frequencies in an InP-Based Waveguide Device with Metamaterial," IEEE J. Quantum Electron. **47**(5), 736–744 (2011).
12. T. Amemiya, T. Shindo, D. Takahashi, S. Myoga, N. Nishiyama, and S. Arai, "Nonunity permeability in metamaterial-based GaInAsP/InP multimode interferometers," Opt. Lett. **36**(12), 2327–2329 (2011).
13. K. L. Tsakmakidis, A. D. Boardman, and O. Hess, "'Trapped rainbow' storage of light in metamaterials," Nature **450**(7168), 397–401 (2007).
14. H. Hu, D. Ji, X. Zeng, K. Liu, and Q. Gan, "Rainbow trapping in hyperbolic metamaterial waveguide," Sci. Rep. **3**(1), 1249 (2013).
15. T. Amemiya, A. Ishikawa, T. Kanazawa, J. Kang, N. Nishiyama, Y. Miyamoto, T. Tanaka, and S. Arai, "Permeability-controlled optical modulator with Tri-gate metamaterial: control of permeability on InP-based photonic integration platform," Sci. Rep. **5**(1), 8985 (2015).
16. Z. J. Wong, Y.-L. Xu, J. Kim, K. O'Brien, Y. Wang, L. Feng, and X. Zhang, "Lasing and anti-lasing in a single cavity," Nat. Photonics **10**(12), 796–801 (2016).
17. Z. Li, M.-H. Kim, C. Wang, Z. Han, S. Shrestha, A. C. Overvig, M. Lu, A. Stein, A. M. Agarwal, M. Lončar, and N. Yu, "Controlling propagation and coupling of waveguide modes using phase-gradient metasurfaces," Nat. Nanotechnol. **12**(7), 675–683 (2017).
18. R. Guo, M. Decker, F. Setzpfandt, X. Gai, D.-Y. Choi, R. Kiselev, A. Chipouline, I. Staude, T. Pertsch, D. N. Neshev, and Y. S. Kivshar, "High-bit rate ultra-compact light routing with mode-selective on-chip nanoantennas," Sci. Adv. **3**(7), e1700007 (2017).
19. M. J. R. Heck, H.-W. Chen, A. W. Fang, B. R. Koch, D. Liang, H. Park, M. N. Sysak, and J. E. Bowers, "Hybrid Silicon Photonics for Optical Interconnects," IEEE J. Sel. Top. Quantum Electron. **17**(2), 333–346 (2011).
20. J. K. Doylend and A. P. Knights, "The evolution of silicon photonics as an enabling technology for optical interconnection," Laser Photonics Rev. **6**(4), 504–525 (2012).
21. K. Totsuka, N. Kobayashi, and M. Tomita, "Slow light in coupled-resonator-induced transparency," Phys. Rev. Lett. **98**(21), 213904 (2007).
22. T. Baba, "Slow light in photonic crystals," Nat. Photonics **2**(8), 465–473 (2008).
23. S. Yamasaki, T. Amemiya, Z. Gu, J. Suzuki, N. Nishiyama, and S. Arai, "Analysis of the slow-light effect in silicon wire waveguides with metamaterials," J. Opt. Soc. Am. B **35**(4), 797–804 (2018).
24. J. Zhou, T. Koschny, M. Kafesaki, E. N. Economou, J. B. Pendry, and C. M. Soukoulis, "Saturation of the magnetic response of split-ring resonators at optical frequencies," Phys. Rev. Lett. **95**(22), 223902 (2005).
25. T. Amemiya, S. Myoga, T. Shindo, E. Murai, N. Nishiyama, and S. Arai, "Permeability retrieval in InP-based waveguide optical device combined with metamaterial," Opt. Lett. **37**(12), 2301–2303 (2012).
26. T. Amemiya, T. Kanazawa, S. Yamasaki, and S. Arai, "Metamaterial Waveguide Devices for Integrated Optics," Materials (Basel) **10**(9), 1037 (2017).
27. Y. A. Vlasov, M. O'Boyle, H. F. Hamann, and S. J. McNab, "Active control of slow light on a chip with photonic crystal waveguides," Nature **438**(7064), 65–69 (2005).
28. T. Amemiya, S. Yamasaki, M. Tanaka, H. Kagami, K. Masuda, N. Nishiyama, and S. Arai, "SD10-buf-10u.xlsx: Raw data for Fig. 8(b)," figshare (2019), https://doi.org/10.6084/m9.figshare.7948337.